HHS Public Access

Author manuscript

*Nat Immunol*. Author manuscript; available in PMC 2014 December 01.

Published in final edited form as:

*Nat Immunol*. 2014 June ; 15(6): 562–570. doi:10.1038/ni.2885.

# USP15 stabilizes MDM2 to mediate cancer cell survival and inhibit antitumor T cell responses

**Qiang Zou**[1], **Jin Jin**[1], **Hongbo Hu**[1], **Haiyan S. Li**[1], **Simona Romano**[1,4], **Yichuan Xiao**[1], **Mako Nakaya**[1], **Xiaofei Zhou**[1], **Xuhong Cheng**[1], **Peirong Yang**[2], **Guillermina Lozano**[2,3], **Chengming Zhu**[1,3], **Stephanie S. Watowich**[1,3], **Stephen E Ullrich**[1,3], and **Shao-Cong Sun**[1,3]

[1]Department of Immunology The University of Texas MD Anderson Cancer Center, 7455 Fannin Street, Box 902, Houston TX 77030, USA.

[2]Department of Genetics, The University of Texas MD Anderson Cancer Center, 7455 Fannin Street, Box 902, Houston TX 77030, USA.

[3]The University of Texas Graduate School of Biomedical Sciences, Houston, TX 77030, USA.

[4]Department of Molecular Medicine and Medical Biotechnologies, Federico II University, Naples, Italy

## Abstract

Deubiquitinases (DUBs) represent a new class of drug targets, although the physiological function of only few DUBs has been characterized. Here we identified the DUB USP15 as a crucial negative regulator of T cell activation. USP15 stabilized an E3 ubiquitin ligase, MDM2, which in turn negatively regulated T cell activation by targeting the degradation of the transcription factor NFATc2. USP15 deficiency promoted T cell activation *in vitro* and enhanced T cell responses to bacterial infection and tumor challenge *in vivo*. USP15 also stabilized MDM2 in cancer cells and regulated p53 function and cancer cell survival. Our results suggest that inhibition of USP15 may both induce tumor cell apoptosis and boost antitumor T cell responses.

### Keywords

Deubiquitinase; USP15; MDM2; T-cell activation; tumorigenesis

Ubiquitination is an important protein modification that regulates diverse biological and pathological processes, including immune responses and oncogenesis[1, 2]. A major function of ubiquitination is to target proteins to the proteasome for degradation, but many nondegradative functions have also been characterized [3, 4]. Ubiquitin conjugation is mediated by the sequential action of three enzymes, the ubiquitin-activating enzyme (E1),



**AUTHOR CONTRIBUTIONS** Q.Z. designed and performed the experiments, prepared the figures, and wrote part of the manuscript; J.J., H.H., H.S.L., S.R., Y.X., M.N., X.Z., X.C., P.Y. and C.Z. contributed to the performance of the experiments; S.S.W. and G.L were involved in supervision of H.S.L. and P.Y., respectively; SEU was involved in collaboration on cancer model studies, and S.-C.S. supervised the work and wrote the manuscript.

**COMPETING FINANCIAL INTERESTS** The authors declare no competing financial interests.

the ubiquitin-conjugating enzymes (E2s) and the ubiquitin ligases (E3s) [3]. Different types of polyubiquitin chains can be formed through connection of the C-terminal glycine of a ubiquitin to any one of the 7 internal lysine residues of the preceding ubiquitin[5]. Lysine (K) 48-linked polyubiquitin chains are the best-studied ubiquitin chains that target proteins for proteasomal degradation, whereas some other ubiquitin chains, such as the K63-linked polyubiquitin chains, can mediate nondegradative functions[4]. The specificity of protein ubiquitination is regulated by the E3 ubiquitin ligases, which exist in large numbers in mammalian cells and mediate substrate recognitions [3, 6].

The E3 ubiquitin ligase MDM2 has been extensively studied as an oncogene product that mediates the ubiquitin-dependent degradation and functional inactivation of the tumor suppressor p53[7, 8]. Elevated MDM2 protein expression was documented in a large variety of human cancers and thought to be due to gene amplification as well as transcriptional and posttranslational regulation. Although the best-characterized target of MDM2 is p53, MDM2 has additional substrates[7]. Small-molecule inhibitors of MDM2, which block MDM2-p53 interaction or inhibit the ubiquitin ligase activity of MDM2, have been actively investigated in preclinical studies and clinical trails for the treatment of cancer [8, 9]. Compared to the extensive studies of MDM2 in cancer cells, its physiological role is relatively poorly understood. In particular, how MDM2 regulates immune responses is largely unclear.

Ubiquitination is a reversible reaction, since the ubiquitin chains can be cleaved by a large family of ubiquitin-specific proteases, termed deubiquitinases (DUBs)[10, 11]. DUBs can have specificity for both protein substrates and ubiquitin chains and, thereby, bring in a different level of diversity in the regulation of ubiquitination. Like the E3 ubiquitin ligases, DUBs regulate diverse biological processes and represent a new class of drug targets[12-14]. However, the biological function of only a small proportion of DUBs has so far been characterized using physiological models, hampering the development of DUB-based therapies. USP15 is a DUB that belongs to the ubiquitin-specific protease family[15]. *In vitro* studies have implicated USP15 in the regulation of TGF-β signaling and cancer cell survival in cell line models[16-18]. However, the physiological role of USP15, particularly the regulation of immune functions, has remained unclear. The molecular mechanism underlying the signaling function of USP15 is also incompletely understood.

In the present study, we studied the function of USP15 using gene-targeting approach and identified USP15 as a negative regulator of T cell activation as well as a pivotal mediator of cancer cell survival. We present biochemical and genetic evidence that USP15 functions by stabilizing the E3 ubiquitin ligase MDM2. In both activated T cells and cancer cells, loss of USP15 caused MDM2 degradation. MDM2 targets a T cell transcription factor, NFATc2, and negatively regulates T cell activation. USP15 deficiency promoted T cell responses to both bacterial infections and tumor cell challenge. In cancer cells USP15 stabilized MDM2 and regulated p53 responses. These results suggest that targeting USP15 may both induce tumor cell apoptosis and boost antitumor T cell responses and, thus, have important clinical applications.

# RESULTS

## USP15 is a negative regulator of T cell activation

Through analyses of the BioGPS database, we found that USP15 was abundantly expressed in immune cells (data not shown). We employed a gene targeting approach to investigate the physiological function of USP15 (Supplementary Fig. 1a-d). The USP15 homozygous knockout (KO) mice (*Usp15*$^{-/-}$) mice were born with expected Mendelian ratios and had comparable survival rate as the wild-type control mice (Supplementary Fig. 1e). The *Usp15*$^{-/-}$ mice also did not show obvious abnormalities in thymocyte development or peripheral T cell homeostasis (Supplementary Fig. 1f-i). However, the USP15 deficiency promoted the TCR+CD28-stimulated production of cytokines, such as interleukin 2 (IL-2) and interferon-γ (IFN-γ), in naïve CD4$^+$ T cells, as assessed by quantitative real-time RT-PCR (qRT-PCR) (Fig. 1a), intracellular cytokine staining (Fig. 1b) and ELISA (Fig. 1c). The loss of USP15 did not reduce the threshold of T cell responses, but appeared to enhance the cytokine induction at different doses of TCR+CD28 stimulation (Fig. 1d). Induction of the effector T cell marker CD44, although not of the early activation marker CD69, was also enhanced in the USP15-deficient T cells (Fig. 1e and data not shown). To examine whether USP15 has a T cell intrinsic function in regulating T cell activation, we reconstituted USP15-deficient T cells with USP15 by retroviral infection of T cell-depleted *Usp15*$^{-/-}$ bone marrow cells and adoptive transfer into *Rag1*$^{-/-}$ mice (Supplementary Fig. 2a). Naïve CD4$^+$ T cells derived from the USP15-reconstituted bone marrow cells displayed reduced IFN-γ induction (Supplementary Fig. 2b). In contrast, reconstitution of the cells with a catalytically inactive USP15 mutant, C298A[19], failed to suppress the induction of IFN-γ-producing cells (Supplementary Fig. 2b). Thus, USP15 negatively regulates T cell cytokine production via its DUB function.

We next examined the role of USP15 in the regulation of CD4$^+$ T cell differentiation by stimulating naïve CD4$^+$ T cells under $T_H1$ (10 μg/ml anti-IL4, 10 ng/ml IL-12), $T_H2$ (10 μg/ml anti-IFN-γ, 20 ng/ml IL-4), $T_H17$ (10 μg/ml anti-IL4, 10 μg/ml anti-IFN-γ, 15 ng/ml IL-6, 2.5 ng/ml TGF-β) and inducible regulatory T ($iT_{reg}$) (10 μg/ml anti-IL4, 10 μg/ml anti-IFN-γ, 1.5 ng/ml TGF-β) cell conditions. Under these standard T cell differentiation conditions, USP15-deficient and wild-type T cells were similar in differentiation and proliferation, although the USP15-deficient T cells had moderately enhanced apoptosis compared to wild-type T cells (Supplementary Fig. 2c-e). However, in the presence of suboptimal doses (0.1 and 1 ng/ml) of IL-12 of $T_H1$ differentiation conditions, *Usp15*$^{-/-}$ CD4$^+$ T cells showed enhanced $T_H1$ differentiation (Fig. 1f). We also examined if USP15-deficient naïve CD4$^+$ T cells showed altered differentiation into $iT_{reg}$. In the presence of a low concentration (0.5 ng/ml) of TGF-β and in the absence of an IFN-γ-blocking antibody, *Usp15*$^{-/-}$ naïve CD4$^+$ T cells did not efficiently differentiate into $iT_{reg}$ cells; however, the USP15-deficient naïve CD4$^+$ T cells differentiated into iTreg cells normally in the presence of the IFN-γ-blocking antibody or a higher dose (1.5 ng/ml) of TGF-β (Supplementary Fig. 2f). Moreover, wild-type and *Usp15*$^{-/-}$ mice had comparable frequencies of $T_{reg}$ cells in peripheral lymphoid organs and thymus (Supplementary Fig. 2g). Collectively, these results suggest that USP15 negatively regulates naïve CD4$^+$ T cell activation and $T_H1$ differentiation.

### USP15 inhibits T cell responses to *Listeria* infection

To examine the *in vivo* role of USP15 in the regulation of T cell responses, we employed a bacterial infection model known to induce strong T cell responses, particularly IFN-γ-producing $CD4^+$ T cells[20]. In response to *Listeria monocytogenes* (*L. monocytogenes*) infection, both the wild-type and the $Usp15^{-/-}$ mice generated IFN-γ-producing $CD4^+$ T cells specific for the listeriolysin O (LLO) antigen (Fig. 2a). However, the $Usp15^{-/-}$ mice had a higher frequency and absolute numbers of IFN-γ-producing $CD4^+$ T cells than the wild-type mice, although the IFN-γ median fluorescence intensity (MFI) of the IFN-$\gamma^+$ T cells was comparable between the two genotypes (Fig. 2a and Supplementary Fig. 3a,b). Moreover, the serum concentration of IFN-γ was significantly increased in *L. monocytogenes*-infected $Usp15^{-/-}$ mice compared to wild-type mice (Fig. 2b). Consistent with their heightened T cell responses, the $Usp15^{-/-}$ mice had a significantly lower bacterial load in the liver (Fig. 2c).

To examine the $CD4^+$ T cell-intrinsic function of USP15, we reconstituted T cell-deficient $Tcrb/d^{-/-}$ mice with wild-type or $Usp15^{-/-}$ naïve $CD4^+$ T cells along with an equal number of wild-type $CD8^+$ T cells. We did not detect differences in the spleen size or numbers of splenic $CD4^+$ T cells between wild-type- and $Usp15^{-/-}$ -reconstituted hosts under uninfected conditions after 4 days of T cell transfer (Supplementary Fig. 3c-e). However, following *L. monocytogenes* infection, $Usp15^{-/-}$ T cells-reconstituted hosts had stronger immune responses, as indicated by a more profound spleen enlargement (Supplementary Fig. 3f), increased numbers of splenic $CD4^+$ T cells (Fig. 2d) and elevated serum IFN-β (Fig. 2e) compared to host reconstituted with wild-type T cells. The *L. monocytogenes*-infected recipients of $Usp15^{-/-}$ T cell also had significantly higher numbers splenic $CD11b^+$ monocytes and $CD11c^+$ dendritic cells, consistent with increased activation and recruitment of myeloid cells by T cell derived cytokines (Supplementary Fig. 3g). Correlating with stronger immune responses, the $Usp15^{-/-}$ T cell reconstituted hosts had reduced bacterial load in the liver (Fig. 2f) and increased survival rate (Fig. 2g).

Because the *L. monocytogenes* strain used in our studies encodes chicken ovalbumin ((LM-OVA), we crossed the $Usp15^{-/-}$ mice with OT-II mice, which express a transgenic TCR specific for an OVA peptide, to generate $Usp15^{-/-}$ OT-II and $Usp15^{+/+}$ OT-II littermate control mice. To test the effect of the USP15 deficiency on antigen-specific $CD4^+$ T cell responses, we adoptively transferred naïve $CD4^+$ T cells isolated from $Usp15^{-/-}$ OT-II and $Usp15^{+/+}$ OT-II littermates into B6.SJL mice and tracked donor and host T cells based on the expression of the congenic markers CD45.2 and CD45.1, respectively. In response to LM-OVA infection, recipients of $Usp15^{-/-}$ OT-II T cells produced a higher frequency (Fig. 2h,i) and absolute numbers (Fig. 2j) of OVA-specific IFN-γ-producing OT-II T cells than mice receiving $Usp15^{+/+}$ OT-II T cells. Moreover, the mice receiving $Usp15^{-/-}$ OT-II T cells also had higher numbers of total splenic $CD45.2^+$ T cells than the mice receiving $Usp15^{+/+}$ OT-II T cells upon LM-OVA challenge, suggesting increased expansion of the $Usp15^{-/-}$ OT-II T cells (Supplementary Fig. 3h). On the other hand, the number of $T_{reg}$ cells was similar in the recipients of $Usp15^{-/-}$ OT-II and $Usp15^{+/+}$ OT-II T cells (Supplementary Fig. 3i). Consistent with their T cell hyper-activation, mice transferred with $Usp15^{-/-}$ OT-II T cells had lower *L. monocytogenes* load in the liver, suggesting a higher ability to clear the

bacteria (Fig. 2k). These results suggest that USP15 is a negatively regulator of $CD4^+$ $T_H1$ responses.

## USP15 deficiency enhances NFATc2 activation in naïve $CD4^+$ T cells

T cell activation involves cascades of signaling events triggered by the TCR and CD28[21]. Upon stimulation with anti-CD3 plus anti-CD28, the *Usp15*$^{-/-}$ and wild-type naïve $CD4^+$ T cells displayed similar TCR-proximal signaling events, including phosphorylation of the protein tyrosine kinases Lck and Zap70 (Supplementary Fig. 4a), and downstream signaling events, such as phosphorylation of the MAP kinase ERK, the kinase AKT or the ribosomal S6 protein (Supplementary Fig. 4b). Furthermore, although USP15 has been implicated as a mediator of TGF-β signaling in certain cancer cell lines[17, 18], USP15-deficient T cells had normal TGF-β signaling, as evidenced by the comparable Smad phosphorylation, upregulation of *Smad7* and downregulation of *Myc* in TGF-β-stimulated wild-type and *Usp15*$^{-/-}$ T cells (Supplementary Fig. 4c,d). Consistently, the wild-type and *Usp15*$^{-/-}$ T cells were both sensitive to TGF-β-mediated suppression of *Il2* and *Ifng* mRNA induction by anti-CD3 plus anti-CD28 (Supplementary Fig. 4e,f). Following TCR+CD28 stimulation, USP15-deficient T cells showed increased nuclear expression of the transcription factor NFATc2 (Fig. 3a), which mediates the induction of T cell specific cytokines[22, 23]. The enhanced induction of NFATc2 nuclear expression in USP15-deficient T cells was not inhibited by TGF-β (Supplementary Fig. 4g). Activation of NFATc1 and two major NF-κB members, c-Rel and p65, was similar in *Usp15*$^{-/-}$ and wild-type T cells following TCR +CD28 stimulation (Fig. 3a). Overexpression of NFATc2 in EL4 T cells promoted the induction of IL-2 and IFN-γ (Supplementary Fig. 4h-j). To further examine the function of NFATc2 in mediating cytokine induction in *Usp15*$^{-/-}$ naïve $CD4^+$ T cells, we employed a bone marrow adoptive transfer approach. We transduced T cell-depleted *Usp15*$^{-/-}$ bone marrow cells with a GFP-expressing lentiviral vector encoding a control or *Nfatc2*-specific shRNA and adoptively transferred the transduced cells into *Rag1*$^{-/-}$ mice. The naïve $CD4^+$ T cells derived from the NFATc2-knockdown bone marrow cells expressed lower levels of IFN-γ protein and mRNA and IL-2 mRNA than the naïve $CD4^+$ T cells derived from the control shRNA-knockdown bone marrow cells (Fig. 3b,c).

We tested if the hyper-activation of NFATc2 in *Usp15*$^{-/-}$ T cells was due to enhanced nuclear translocation, expression or stabilization of NFATc2. Immunoblot assays revealed comparable cytoplasmic expression of NFATc2 in activated wild-type and *Usp15*$^{-/-}$ T cells, despite their increased nuclear expression of NFATc2 (Fig. 3a). Consistently, the whole-cell level of NFATc2 was higher in activated USP15-deficient T cells compared to activated wild-type T cells (Fig. 3d). USP15 deficiency did not enhance *Nfatc2* mRNA induction, as revealed by a qRT-PCR assay (Supplementary Fig. 4k). These results suggested that USP15 might regulate the stability of NFATc2. To examine this possibility, we stimulated T cells in the presence of a protein synthesis inhibitor, cycloheximide (CHX). CHX treatment led to substantial loss of NFATc2 in wild-type, but not in the *Usp15*$^{-/-}$ T cells (Fig. 3e), suggesting that USP15 regulates the degradation of NFATc2. Consistently, blocking protein degradation with a proteasome inhibitor, MG132, resulted in NFATc2 accumulation in wild-type T cells similar to that observed in USP15-deficient T cells (Fig. 3f). We also observed abundant ubiquitination of NFATc2 in the activated wild-type T cells following MG132

treatment, but not in activated *Usp15*$^{-/-}$ T cells (Fig. 3g). Of note, NFATc2 ubiquitination was very low in both wild-type and the *Usp15*$^{-/-}$ T cells under resting conditions, and could only be detected after extended immunoblot exposure (Fig. 3g and data not shown). These data suggest that USP15 promotes the ubiquitination and degradation of activated NFATc2. Because NFATc2 is critical for mediating induction of T cell cytokines, including IL-2 and IFN-γ[22, 23], these results provide a mechanistic insight for the increased production of cytokines in *Usp15*$^{-/-}$ T cells.

## USP15 regulates the stability of the E3 ubiquitin ligase MDM2

Because USP15 is a DUB, we investigated if USP15 acts through regulating an E3 ubiquitin ligase of NFATc2. The E3 ubiquitin ligase MDM2 is known to induce NFATc2 ubiquitination in a breast cancer cell line[24]. Overexpression of MDM2 induced strong ubiquitination of NFATc2 in HEK293 cells (Fig. 4a). To assess the role of MDM2 in T cells, we examined whether T cell activation altered the level of MDM2 expression and whether MDM2 is regulated by USP15. Stimulation of naïve CD4$^+$ T cells by anti-CD3 plus anti-CD28 triggered the induction of *Mdm2* mRNA, which was similar in USP15-deficient and wild-type T cells (Fig. 4b). While TCR-CD28 stimulation induced a transient loss of MDM2 protein in the wild-type naïve CD4$^+$ T cells, this effect was enhanced and prolonged in the *Usp15*$^{-/-}$ naïve CD4$^+$ T cells (Fig. 4c). The proteasome inhibitor MG132 prevented the loss of MDM2 (Fig. 4d) and caused accumulation of ubiquitinated MDM2 with K48-linked polyubiquitin chains in *Usp15*$^{-/-}$ naïve CD4$^+$ T cells (Fig. 4e). These results suggest that USP15 prevents the ubiquitin-dependent degradation of MDM2 in activated T cells.

We next examined whether USP15 directly targets MDM2. When co-expressed in HEK293 cells, USP15 interacted with MDM2, as detected by co-IP assays (Fig. 4f). USP15 contains several structural domains, including a large catalytic domain that covers about 2/3 of the molecule, a DUSP (domain present in ubiquitin-specific protease) and two ubiquitin-like (Ubl) domains, one of which is located within the catalytic domain[25] (Fig. 4f). Domain mapping studies revealed that 2 USP15 C-terminal truncation mutants, 1-941 and 1–583, lacking different lengths of the catalytic domain retained the ability to bind MDM2 (Fig. 4f). An N-terminal truncation mutant, 114–981, lacking the DUSP was also able to bind MDM2, but several other USP15 mutants (278–981, 470–981, and 580–981) with larger N-terminal truncations failed to bind MDM2 (Fig. 4f). These results suggested that the first Ubl domain of USP15 was important for its interaction with MDM2. Endogenous USP15 and MDM2 also formed a stable complex in naïve CD4$^+$ T cells, and this molecular interaction was not influenced by the TCR and CD28 signals (Fig. 4g). USP15-MDM2 association was also detected in p53-deficient T cells (Fig. 4h). Both USP15 and MDM2 were predominantly located in the cytoplasm of naïve CD4$^+$ T cells, where they formed a complex (Supplementary Fig. 5a). MDM2 was located in the cytoplasm in *Usp15*$^{-/-}$ T cells as well (Supplementary Fig. 5b). When we examined the subcellular localization of p53, this protein was barely detectable by IB in untreated naïve CD4$^+$ T cells (data not shown). However, we detected it in the cytoplasm and, to a lesser extent, in the nucleus, following MG132 treatment (Supplementary Fig. 5c). TCR+CD28 stimulation enhanced the amount of nuclear p53. These results suggest that USP15 physically interacts with MDM2 in a p53-independent manner.

Considering the USP15-MDM2 direct association and the role of USP15 in stabilizing MDM2 and inhibiting MDM2 ubiquitination in activated T cells (Fig. 4c-e), we examined whether USP15 directly deubiquitinates MDM2. MDM2 was abundantly ubiquitinated when overexpressed in HEK293 cells, likely throrugh autoubiquitination (Fig. 4i). When cotransfected with wild-type USP15, but not the catalytically inactive USP15 mutant (C298A), the ubiquitination of MDM2 was potently inhibited (Fig. 4i). A parallel HEK293 transfection experiment revealed that USP15 did not inhibit the ubiquitination of NFATc2 (Supplementary Fig. 5d). In addition, USP15 directly deubiquitinated MDM2 *in vitro*, and this required the catalytic activity of USP15 (Fig. 4j). Thus, USP15 appears to be a deubiquitinase of MDM2 that prevents ubiquitin-dependent MDM2 degradation.

## MDM2 negatively regulates NFATc2 and T cell activation

Because MDM2 induced NFATc2 ubiquitination in transfected cells (Fig. 4a), we tested whether endogenous MDM2 regulated the activation or the expression of NFATc2. We found that activation of wild-type T cells in the presence of a small-molecule inhibitor (HLI373), which blocks the ubiquitin ligase activity of MDM2[26], enhanced the accumulation of NFATc2 in the nucleus (Fig. 5a). The MDM2 inhibitor did not affect the activation of several other transcription factors. Furthermore, HLI373 increased the amount of NFATc2 in the cell (Fig. 5b) and caused hyper-induction of IL-2 and IFN-γ in wild-type T cells (Fig. 5c). In contrast, HLI373 did not appreciably enhance NFATc2 activation or cytokine induction in *Usp15*$^{-/-}$ T cells (Supplementary Fig. 5e, f), further suggesting that the USP15 deficiency causes T cell hyperactivation via downregulation of MDM2 (Fig. 4c).

To directly examine whether the lower MDM2 expression in USP15-deficient T cells contributed to the enhanced NFATc2 activation and cytokine induction, we used bone marrow adoptive transfer to express MDM2 in *Usp15*$^{-/-}$ T cells. We transduced T cell-depleted *Usp15*$^{-/-}$ bone marrow cells with a GFP-expressing retroviral vector or a vector encoding MDM2 and adoptively transferred the cells into *Rag1*$^{-/-}$ mice. Expression of the exogenous MDM2 substantially reduced TCR+CD28-stimulated nuclear accumulation of NFATc2 and IFN-γ production (Supplementary Fig. 5g-i). Using the same approach, we found that reconstitution of *Usp15*$^{-/-}$ naïve CD4$^{+}$ T cells with wild-type USP15, but not its mutant C298A, prevented TCR+CD28-induced MDM2 loss and reduced NFATc2 activation (Supplementary Fig. 5j), thus further emphasizing a cell-intrinsic role for USP15 in regulating MDM2 and NFATc2.

Although MDM2 is known as an inhibitor of p53[27], MDM2 deficiency promoted NFATc2 accumulation and cytokine induction even in p53-deficient T cells, suggesting the role of MDM2 in T cell regulation was independent of p53 (Fig. 5d-f). Furthermore, another MDM2 inhibitor, Nutlin3, known to block the MDM2-p53 interaction without inhibiting the overall ubiquitin ligase activity of MDM2[7, 28] did not promote the activation of NFATc2 or the induction of cytokines in wild-type naïve CD4$^{+}$ T cells, although Nutlin-3 did enhance the induction of the p53 target gene p21 (Supplementary Fig. 5k,l). These results suggest that MDM2 negatively regulates NFATc2 activation and cytokine induction in naïve CD4$^{+}$ T cells in a p53-independent manner.

We also noticed that wild-type $CD8^+$ T cells had markedly lower expression of MDM2 than $CD4^+$ T cells, which was due to reduced *Mdm2* mRNA expression (Supplementary Fig. 6a,b). Consistently, unlike the effect seen in naïve $CD4^+$ T cells, USP15 deficiency did not appreciably affect NFATc2 activation or cytokine production in naïve $CD8^+$ T cells (Supplementary Fig. 6c-e), further emphasizing the role of MDM2 in the negative regulation of NFATc2 activation and cytokine induction in T cells. Together, these results suggest that MDM2 functions as a negative regulator of NFATc2 in naïve CD4+ T cells.

## USP15 regulates MDM2 in cancer cells

USP15 is overexpressed in cancer cell lines, although its role in MDM2 regulation in these malignant cells has not been investigated[18, 29]. We found that USP15 was abundantly expressed in most of the melanoma and colorectal cancer cell lines analyzed (Supplementary Fig. 7a). We examined the role of USP15 in the regulation of MDM2 stability and cancer cell survival using two different cancer cell lines, the melanoma cell line A375 and the colorectal cancer cell line HCT116, both expressing wild-type p53[30, 31]. Remarkably, USP15 knockdown in A375 cells using two different shRNAs caused spontaneous reduction in MDM2 protein expression (Fig. 6a) without reducing the level of *Mdm2* mRNA (Fig. 6b). This phenotype differed from the degradation of MDM2 in primary T cells, which required the TCR+CD28 signals (Fig. 4c). The spontaneous degradation of MDM2 appears to be specific for tumor cells, because MDM2 protein was only slightly reduced in USP15-knockdown human primary fibroblasts (Supplementary Fig. 7b) and not changed in *Usp15*$^{-/-}$ murine B cells or thymocytes (Supplementary Fig. 7c).

In the melanoma and colorectal tumor cell lines analyzed, expression of NFATc2 was very low (data not shown). However, MDM2 downregulation in cells in which USP15 was knocked down resulted in upregulation of p53 and its target genes p21 and Puma (Fig. 6a,c), coupled with enhanced apoptosis (Fig. 6d,e). These phenotypes of the USP15 knockdown cells were efficiently reversed upon reconstitution with an RNAi-resistant USP15 expression vector (Supplementary Fig. 7d,e). Knocking down USP15 in the colon cancer cell line HCT116 also caused downregulation of MDM2 and concomitant upregulation of p53 and p53-target genes as well as enhanced apoptosis (Fig. 6f,g). These effects of the USP15 knockdown were dependent on p53, because they were detected in wild-type, but not p53-deficient, HCT116 cells (Supplementary Fig. 7f,g).

Incubation of the USP15-knockdown A375 cells with a proteasome inhibitor (MG132) prevented the loss of MDM2 and caused accumulation of ubiquitinated MDM2 (Fig. 6h and Supplementary Fig. 8a), suggesting that, similar to activated T cells, USP15 was required for preventing ubiquitin-dependent MDM2 degradation in cancer cells. Conversely, incubation of USP15-knockdown HCT116 and A375 cells with CHX, a protein-synthesis inhibitor, resulted in accelerated degradation of MDM2 and delayed degradation of p53 (Supplementary Fig. 8b).

Recent studies suggest a role for USP15 in the regulation of TGF-β signaling in some cancer cell lines[17, 18]. However, knockdown of USP15 in A375 or HCT116 cells did not interfere with TGF-β-stimulated Smad phosphorylation or induction of two TGF-β-target genes, *Pai1* and *Smad7* (Supplementary Fig. 8c-e). These results, together with the finding that USP15

deficiency had no effect on TGF-β signaling in T cells (Supplementary Fig. 4c-g), indicate that the function of USP15 in regulating TGF-β signaling may be cell type specific. Thus, as seen in activated $CD4^+$ T cells, USP15 is required for the stability of MDM2 in A375 melanoma cells and HCT116 colon cancer cells.

### USP15 regulates both tumor growth and anti-tumor immunity

The findings that USP15 deficiency promotes T cell activation and cancer cell apoptosis indicated that inhibition of USP15 might suppress tumor growth both via a tumor cell-intrinsic mechanism and by enhancing the anti-tumor host defense. Knock down of USP15 in A375 and HCT116 cells attenuated the growth of xenograft tumors in nude mice (Fig. 7a and Supplementary Fig. 9a,b). This effect was not seen in p53-deficient HCT116 cells (Supplementary Fig. 9c). Furthermore, introduction of exogenous MDM2 in A375 cells in which USP15 was knocked down reduced the level of p53, promoted tumor growth, and inhibited apoptosis (Fig. 7b-d). We next examined the role of USP15 in regulating anti-tumor host defenses in a B16 melanoma model[32]. Compared to wild-type mice, *Usp15*$^{-/-}$ mice had a profound reduction in B16 tumors size and tumor-induced lethality (Fig. 7e,f). Knocking down USP15 in the B16 cells revealed a combinatorial effect on tumor inhibition (Supplementary Fig. 9d-f). Compared to wild-type hosts, B16-challanged *Usp15*$^{-/-}$ mice had an increased frequency of IFN-$\gamma^+$ $CD4^+$ T cells infiltrating to the tumors (Fig. 7g and Supplementary Fig. 9g). Despite the lack of a direct effect of USP15 deficiency on $CD8^+$ T cell activation (Supplementary Fig. 6), B16-challenged *Usp15*$^{-/-}$ mice also had an increased frequency of tumor-infiltrating $CD8^+$ effector T cells. This is due probably to increased activation and recruitment of $CD8^+$ T cells to tumor site by the $CD4^+$ T cells via different mechanisms, including the production of IFN-γ[33]. We also considered the potential involvement of $T_{reg}$ cells. Wild-type and *Usp15*$^{-/-}$ mice had similar frequencies of $T_{reg}$ cells in both the lymphoid organs and the tumors (Supplementary Fig. 10a,b).

We next examined the role of IFN-γ-producing T cells in mediating tumor suppression. Injection of an IFN-γ neutralizing antibody in the *Usp15*$^{-/-}$ mice promoted tumor growth, suggesting IFN-γ contributes to the stronger anti-tumor immunity in *Usp15*$^{-/-}$ mice (Supplementary Fig. 10c). To examine the T cell-intrinsic function of USP15 in regulating anti-tumor immunity, we reconstituted T cell-deficient *Tcrb/d*$^{-/-}$ mice with wild-type or *Usp15*$^{-/-}$ naïve $CD4^+$ T cells along with wild-type $CD8^+$ T cells and then challenged the recipient mice with B16 melanoma cells. Compared to host receiving wild-type T cells, mice receiving *Usp15*$^{-/-}$ T cells were much more efficient in controlling the melanoma growth (Fig. 7h). When not challenged with the B16 melanoma cells, the mice receiving wild-type and *Usp15*$^{-/-}$ T cells had similar numbers of splenic $CD4^+$ T cells in the spleen (Supplementary Fig. 10d). Together, these findings suggest that USP15 inhibition may not only promote cancer cell apoptosis but also boost T cell-mediated anti-tumor immunity.

## DISCUSSION

Here we identify USP15 as a negative regulator of T cell activation. USP15 deficiency promotes T cell activation *in vitro* and enhances T cell responses *in vivo* to *L. monocytogenes* infection and tumor challenge. USP15 functions to stabilize MDM2, which

in turn mediates ubiquitin-dependent degradation of NFATc2 and negatively regulates T cell activation. USP15 also stabilizes MDM2 in cancer cells and regulates p53 function and cancer cell survival. These findings suggest that targeting USP15 may both induce tumor cell apoptosis and boost antitumor T cell responses.

MDM2 is known as an inhibitor of p53 and a mediator of cancer cell survival; however, the role of MDM2 in the regulation of immune responses has remained poorly understood. Our data suggested a p53-independent function of MDM2 in the regulation of T cell activation. Notably, there are two different types of MDM2 inhibitors, which function by inhibiting the E3 activity of MDM2 and interfering with the MDM2-p53 interaction, respectively. These two different types of MDM2 inhibitors had very different effect on T cell activation, suggesting possible differences in their therapeutic efficacies when used in combination with immunotherapeutic approaches. Since HLI373, but not Nutlin-3, promotes T-cell activation, the former may be ideal for partnering with cancer immunotherapy.

Prior studies suggest that USP15 also regulates TGF-β signaling in certain cancer cell lines[17, 18]. Because TGF-β is an immunosuppressive cytokine, it raises the intriguing question of whether the negative role of USP15 in regulating T cell activation also involves altered TGF-β signaling. However, we were unable to detect an obvious defect of the USP15-deficient $CD4^+$ T cells in TGF-β-stimulated Smad phosphorylation or target gene expression. These data suggest that the function of USP15 in regulating TGF-β signaling may be dependent on cell types and/or activation conditions. Future studies will examine this potential role of USP15 in different types of immune cells.

We found that USP15 mediates the stability of MDM2 in both T cells and cancer cells. USP15 appeared to function as a deubiquitinase of MDM2, because it bound to MDM2 and directly cleaved the ubiquitin chains from MDM2. Loss of USP15 in melanoma and colorectal cell lines caused spontaneous ubiquitination and degradation of MDM2, suggesting that the amount of MDM2 in cancer cells is maintained by a dynamic balance between ubiquitination and deubiquitination. In resting T cells, MDM2 was stable even in the absence of USP15; however, the TCR+CD28 signals stimulated ubiquitin-dependent degradation of MDM2, which was negatively regulated by USP15. How T cell activation signals trigger the degradation of MDM2 remains to be further studied, but one possibility is that the TCR+CD28 signals stimulate the E3 activity of MDM2, causing both MDM2 self-ubiquitination and the ubiquitination of its targets. This hypothesis also explains why NFATc2 undergoes ubiquitination in activated, but not resting, T cells. In addition to USP15, USP7 has been implicated in the regulation of MDM2 in cancer cells. USP7 was originally identified as a DUB that stabilizes p53, but subsequent studies suggest that USP7 also regulates MDM2[34, 35]. It is unknown whether USP7 also regulates immune functions, particularly T cell activation. Another intriguing question is whether USP15 and USP7 functionally cooperate in the regulation of MDM2. A protein-protein interaction screen study has revealed the physical interaction between USP15 and USP7, although the functional significance remains to be further studied[36].

Our findings have important implications for cancer therapy. Immunotherapy and targeted therapy are two promising approaches in the treatment of cancer[37]. It has been suggested

that the combination of these approaches may represent a paradigm shift to greatly improve the clinical efficiencies. However, for the successful partnering of targeted therapy with immunotherapy, it is important that the drug targets are not required for immune functions. Ideally, the anti-cancer drugs should also promote anti-tumor immunity. Our current findings suggest that USP15 may be an excellent drug target for partnering with immunotherapy. Future studies will directly examine this possibility using animal models of cancer therapy.

## ONLINE METHODS

### Mice

*Usp15*$^{-/-}$ mice were generated using the OmniBank retroviral gene-trapping technique (Taconic). The mice were originally in B57BL/6-129 mixed background and subsequently backcrossed for four generations to the C57BL/6 background. *USP15*$^{+/-}$ heterozygous mice were bred to generate wild-type (+/+) and KO (−/−) littermates for experiments. Complete ablation of USP15 was confirmed by both IB assays and RT-PCR to amplify different regions of the *Usp15* mRNA (primers used are listed in Supplementary Table 1). Mice harboring double deletions of the TCR beta and delta genes (*Tcrb/d*$^{-/-}$) and thus completely lacking T cells were obtained from Jackson Lab (in C57BL/6 background). B6.SJL mice (expressing the CD45.1 congenic marker), *Rag1*$^{-/-}$ mice, and the OT-II TCR–transgenic mice (all on C57BL/6 background) were from The Jackson Laboratory. OT-II mice were crossed with the *Usp15*$^{-/-}$ mice to generate *Usp15*$^{-/-}$ OTII and wild-type OT-II control mice. The *p53*$^{-/-}$ mice were from LA Donehower (Baylor College of Medicine) and bred in C57BL6-129 mixed background, and the *p53*$^{-/-}$ *Mdm2*$^{-/-}$ mice were as described [38]. Mice were maintained in specific pathogen-free facility, and all animal experiments were conducted in accordance with protocols approved by the Institutional Animal Care and Use Committee of the University of Texas MD Anderson Cancer Center.

### Plasmids

The retroviral expression vector for human USP15 (double tagged with HA and FLAG) was purchased from Addgene (plasmid #22570) and used as template for creating the catalytically inactive USP15 mutant, C298A, by site-directed mutagenesis. The originally reported USP15 mutant, C269A, was named based on the sequence of USP15 isoform 2 cDNA[19]. This corresponding residue in USP15 isoform 1 is C298. Full-length USP15 isoform 1 and its truncation mutants were subcloned into the HindIII and SalI sites of the p3xFLAG vector by PCR using primers listed in Supplementary Table 2. The expression vectors pcDNA-Xpress-His-USP15 (Addgene, #23216) and pcDNAXpress-His-USP15 C269A (Addgene, #23217) were used for production of recombinant proteins. These vectors encode USP15 isoform 2[19]. The RNAi-resistant USP15 vector was produced by site-directed mutagenesis to introduce sense mutations at the shRNA-binding site of USP15 cDNA. Primers for site-directed mutagenesis are listed in Supplementary Table 3. The USP15 and USP15 C298A (no epitope tag) were cloned into a lentiviral vector. Human MDM2 (HDM2) plasmid, provided by Dr. Wei Gu (Columbia University), was subcloned into the pMIGR1-GFP retroviral vector with an HA tag. Mouse NFATc2 in the GFP-RV-DV retroviral vector was from Addgene. The shRNAs for human and mouse USP15 and

mouse NFATc2 as well as a non-silencing shRNA control (in the pGIPZ lentiviral vector) were from Thermo Scientific. The lentiviral packaging plasmids, and the HA-Ubiquitin vector have been described previously[39].

### Antibodies and reagents

Antibodies used in this study are listed in Supplementary Table 4, and additional antibodies for cell stimulation, immunoblot and flow cytometry were as described[39]. APC-Annexin V, FITC-Annexin V and Propidium Iodide (PI) staining solution were from BD Biosciences. IL-3, IL-6, stem cell factor, and hTGF-β were from R&D Systems, and IL-12 and IL-4 were from PeproTech. His-tagged human USP15 recombinant protein was from Enzo Life Sciences. His-USP15 and His-USP15 C269A proteins were also produced by transfecting HEK293 cells with pcDNA-Xpress-His-USP15 and pcDNA-Xpress-His-USP15 C269A and purified using His60 Ni Resin (Takara). HLI373 was from TOCRIS, and Nutlin-3 was from Cayman [(−)-Nutlin-3]. CHX, Phorbol 12-myristate 13-acetate (PMA), and ionomycin were from Sigma-Aldrich.

### T cell isolation and stimulation

Primary T cells were isolated from the spleen and lymph nodes of young adult mice (6-8 wk old)[40]. Naïve $CD4^+$ and $CD8^+$ T cells were purified by flow cytometric cell sorting based on $CD4^+CD44^{lo}CD62L^{hi}$ and $CD8^+CD44^{lo}$ surface markers, respectively. The cells were stimulated with plate-bound anti-CD3 (1μg/ml) and anti-CD28 (1μg/ml) in replicate wells of 96-well plates ($1 \times 10^5$ cells per well) for ELISA, 12-well plates ($1 \times 10^6$ cells per well) for qRT-PCR, and 6-well plates ($5 \times 10^6$ per well) for IB assays. Where indicated, the cells were acutely stimulated using an antibody crosslinking protocol[39]. For TGF-β stimulation, the T cells were pre-activated for 24 h with anti-CD3 plus anti-CD28, starved for 24 h in low-serum (0.5%) medium, and then stimulated with TGF-β (10 ng/ml).

### $CD4^+$ T cell differentiation

Naive $CD4^+$ T cells were isolated from spleens and lymph nodes and stimulated with plate-bound anti-CD3 (1 μg/ml) and anti-CD28 (1 μg/ml) under $T_H1$ (10 μg/ml anti-IL4, 10 ng/ml IL-12), $T_H2$ (10 μg/ml anti-IFN-γ, 20 ng/ml IL-4), $T_H17$ (10 μg/ml anti-IL4, 10 μg/ml anti-IFN-γ, 15 ng/ml IL-6, 2.5 ng/ml TGF-β) and $T_{reg}$ (10 μg/ml anti-IL4, 10 μg/ml anti-IFN-γ, 1.5 ng/ml TGF-β) conditions. After 5 days of stimulation, the cells were subjected to ICS, ELISA, or qRT-PCR analyses. The cells were also subjected to proliferation assays based on thymidine incorporation and apoptosis assays. In some experiments, different doses of IL-12 and TGF-β were used for the differentiation of $T_H1$ and $T_{reg}$ cells.

### Flow cytometry, cell sorting, and ICS

Suspensions of splenic and lymph node cells were subjected to flow cytometry and cell sorting as described[40] using LSR II (BD Bioscience) and FACSAria (BD Bioscience) flow cytometers, respectively. The data were analyzed using FlowJo software. For ICS, the anti-CD3/anti-CD28-activated T cells were further stimulated for 4 h with PMA plus ionomycin in the presence of monensin and then subjected to intracellular IFN-γ staining and flow cytometry. For analyzing *in vivo* primed antigen-specific T cells, the T cells were stimulated

*in vitro* with the indicated antigenic peptides in the presence of monensin and then subjected to ICS.

### ELISA and qRT-PCR

Supernatants of *in vitro* cell cultures or sera of mice were analyzed by ELISA using a commercial assay system (eBioScience). Total RNA was prepared for the indicated cells and subjected to qRT-PCR[39] using gene-specific primers (Supplementary Table 5).

### IB and ubiquitination assays

Total cell lysates or subcellular extracts were prepared and subjected to IB assays as described[41]. The Santa Cruz anti-USP15 (2D5) and the Proteintech anti-USP15 antibodies were used for detecting human and mouse USP15, respectively. The Millipore anti-MDM2 and the Sigma anti-MDM2 antibodies were used for detecting human and mouse MDM2, respectively. For ubiquitination assays, MDM2 and NF-ATc2 were isolated by IP under denaturing conditions[39], and the ubiquitinated MDM2 and NFATc2 were detected by IB using a ubiquitin antibody specifically detecting K48-linked ubiquitin chains (Millipore). For transfection models, MDM2 or NFATc2 was transfected into HEK293 cells along with HA-ubiquitin, and the ubiquitinated MDM2 and NFATc2 were isolated by denaturing IP and detected by anti-HA IB. For deubiquitination assays, the isolated MDM2–ubiquitin conjugates were incubated with purified USP15 or its catalytic mutant in a deubiquitination buffer[42] for 4 h and then subjected to IB using anti-ubiquitin.

### Cell culture, gene silencing and overexpression

Human melanoma cell line A375 and colon cancer cell line HCT116 were cultured in Dulbecco's modified Eagle's medium (DMEM) supplemented with 10% fetal bovine serum (FBS) and 1% penicillin/streptomycin. HCT116 p53 null ($p53^{-/-}$) and wild-type control ($p53^{+/+}$) cells were provided by Dr. Bert Vogelstein (Johns Hopkins University), and the normal human dermal fibroblasts were from PromoCell. Murine B16 melanoma cells stably transfected with OVA were provided by Dr. Qing Yi[43]. For gene silencing, lentiviral particles were prepared as described[39] by transfecting HEK 293T cells with pLKO.1 or pGIPZ lentiviral vectors encoding specific shRNAs along with packaging plasmids. The packaged viruses were then used to infect the indicated cells, followed by selection of the infected cells by puromycin (1 μg/ml) for 7 days or by sorting $GFP^+$ cells (for the pGIPZ vector). For overexpression studies, lentiviral transduction was as described above, and retroviral packaging and transduction was as described previously[44].

### Bone marrow transduction and adoptive transfer

Bone marrow cells were taken from *Usp15*$^{-/-}$ or wild-type control mice that were treated with 5-fluorouracil (150 mg/kg) for 48 h. After removal of RBCs and $CD90.2^+$ cells, they were cultured in IMDM with 15% FBS in the presence of IL-3 (20 ng/ml), IL-6 (20 ng/ml), and stem cell factor (50 ng/ml) for 3 days. Bone marrow cells were mixed with viral supernatant in the presence of polybrene (8 ng/ml), cultured in the presence of IL-3, IL-6, and stem cell factor for an additional 24 h, and then mixed with viral supernatant again. The efficiency of viral transduction of bone marrow cells was examined by monitoring GFP

expression using fluorescence microscopy. Before adoptive transfer, transduced bone marrow cells were harvested and washed once with IMDM without FBS. A total of $10^6$ cells were injected i.v. via a tail vein into lethally irradiated (950 rad) *Rag1*$^{-/-}$ mice.

## T cell adoptive transfer

Sorted wild-type or *Usp15*$^{-/-}$ naïve CD4$^+$ T cells (CD4$^+$CD44$^-$CD62L$^+$ CD25$^-$) ($5 \times 10^6$) were adoptively transferred, via i.v. injection, into age- and sex-matched *Tcrb/d*$^{-/-}$ mice along with the same number of wild-type CD8$^+$ T cells. After 8 h, the recipient mice were challenged with *L. monocytogenes* or B16 melanoma cells. wild-type or *Usp15*$^{-/-}$ OT-II naïve CD4$^+$ T cells ($5 \times 10^6$) were adoptively transferred, via i.v. injection, into age- and sex-matched B6.SJL mice. After 8 h, the recipient mice were challenged with OVA-expressing *L. monocytogenes.*

## *L. monocytogenes* infection

Recombinant *L. monocytogenes* expressing a truncated OVA protein (LM-OVA) was provided by Dr. Hao Shen via DMX Incorporated[45]. Age- and sex-matched wild-type and *Usp15*$^{-/-}$ mice (8-12 wk old) were infected i.v. with LM-OVA ($5 \times 10^4$ CFU per mouse) and sacrificed after 6 days of infection to analyze the primary host response. Livers were homogenized in 10 ml 0.2% (vol/vol) Nonidet P-40 in PBS, and the organ homogenates were serially diluted and plated on streptomycin agar plates to determine the CFU of *L. monocytogenes*. Splenocytes were collected for flow-cytometric analysis of listeriolysin O (LLO)-specific CD4$^+$ T lymphocytes. In brief, the splenocytes were stimulated with 5 μg/ml of $LLO_{190\text{-}201}$ peptide (*NEKYAQAYPNVS*) in the presence of monesin, followed by intracellular IFN-γ staining and flow cytometry analysis. LM-OVA infection was also carried out using the T cell-transferred *Tcrb/d*$^{-/-}$ mice, followed by analyzing immune cell activation as described above. We found that these mice (especially those transferred with wild-type CD4$^+$ T cells) had a high rate of lethality when infected at the regularly used dose ($5 \times 10^4$ CFU per mouse) and therefore used a lower dose ($5 \times 10^3$ CFU per mouse) for analyzing the liver bacterial loads.

The B6.SJL mice, adoptively transferred with wild-type or *Usp15*$^{-/-}$ OT-II naïve CD4$^+$ T cells, were infected i.v. with LM-OVA ($5 \times 10^4$ CFU per mouse) as described above. Splenocytes were stimulated with 5 μg/ml of $OVA_{323\text{-}339}$ peptide, and the IFN-γ-producing OT-II T cells were detected by ICS and flow cytometry based on their expression of the CD45.2 congenital marker.

## Analysis of apoptosis

Apoptotic cells were measured based on nuclear staining with PI[46]. Briefly, the cells were incubated for 0.5 h in a hypotonic PI-staining buffer (0.1% sodium citrate, 0.1% Triton X-100, and 50 μg/ml PI) and then subjected to flow cytometry to quantify the apoptotic/necrotic cell population (sub-G1/G0 cell fraction). Early-stage apoptosis was determined by FITC-annexin V staining (BD Biosciences), based on the translocation of phosphatidylserine to the extracellular membrane leaflet in apoptotic cells.

### B16 model of melanoma and human cancer xenograft studies

wild-type and *Usp15*$^{-/-}$ mice were injected s.c. with $5 \times 10^5$ B16 melanoma cells expressing a surrogate tumor antigen, OVA. The challenged mice were monitored for tumor growth, and the mice were sacrificed when their tumor size reached 225 $mm^2$ based on protocols approved by the Institutional Animal Care and Use Committee of the University of Texas MD Anderson. Thus, lethality was defined as tumor size reaching to 225 $mm^2$. To minimize individual variations, littermate wild-type and *Usp15*$^{-/-}$ mice were used. For the human cancer xenograft study, female nude (nu/nu) mice (8 wk old) were injected s.c. with $1 \times 10^7$ A375 human melanoma cells or HCT116 human colorectal cell line and monitored for tumor growth. Mice were randomly selected for tumor injection. Analysis of tumor size was done blindly by one examiner with the results confirmed by a second blinded examiner.

### Statistical analysis

Statistical analysis was performed using Prism software. Two-tailed unpaired *t*-tests were performed and *P* values less than 0.05 were considered significant, and the level of significance was indicated as *P<0.05 and **P<0.01. In the animal studies, 4 mice are required for each group based on the calculation to achieve a 2.3 fold change (effect size) in two-tailed *t* -test with 90% power and a significance level of 5%. All statistical tests are justified as appropriate, and data meet the assumptions of the tests. The variance is similar between the groups being statistically compared.

## Supplementary Material

Refer to Web version on PubMed Central for supplementary material.

## ACKNOWLEDGEMENTS

We thank W Gu for expression vectors, BV for HCT116 derivative cell lines, S. Hao for recombinant *L. monocytogenesis*, Q Yi for B16 cell line, and LA Donehower for p53$^{-/-}$ mice. We also thank the personnel from the NIH/NCI-supported resources (flow cytometry, DNA analysis, and animal facilities) under award number P30CA016672 at The MD Anderson Cancer Center. This study was supported by grants from the National Institutes of Health (AI057555, AI064639, GM84459, and AI104519 to SCS and AI098099 to SSW) and partially supported by a Sister Institution Network Fund and a seed fund from the Center for Inflammation and Cancer at the MD Anderson Cancer Center.

## REFERENCES

1. Liu YC, Penninger J, Karin M. Immunity by ubiquitylation: a reversible process of modification. Nat. Rev. Immunol. 2005; 5:941–952. [PubMed: 16322747]
2. Lipkowitz S, Weissman AM. RINGs of good and evil: RING finger ubiquitin ligases at the crossroads of tumour suppression and oncogenesis. Nat. Rev. Cancer. 2011; 11:629–643. [PubMed: 21863050]
3. Hershko A, Ciechanover A. The ubiquitin system. Annu. Rev. Biochem. 1998; 67:425–479. [PubMed: 9759494]
4. Chen ZJ, Sun LJ. Nonproteolytic functions of ubiquitin in cell signaling. Mol. Cell. 2009; 33:275–286. [PubMed: 19217402]
5. Kulathu Y, Komander D. Atypical ubiquitylation - the unexplored world of polyubiquitin beyond Lys48 and Lys63 linkages. Nat. Rev. Mol. Cell. Biol. 2012; 13:508–523. [PubMed: 22820888]

6. Li W, et al. Genome-wide and functional annotation of human E3 ubiquitin ligases identifies MULAN, a mitochondrial E3 that regulates the organelle's dynamics and signaling. PLoS One. 2008; 3:e1487. [PubMed: 18213395]
7. Li Q, Lozano G. Molecular pathways: targeting Mdm2 and Mdm4 in cancer therapy. Clin. Cancer Res. 2013; 19:34–41. [PubMed: 23262034]
8. Wade M, Li YC, Wahl GM. MDM2, MDMX and p53 in oncogenesis and cancer therapy. Nat. Rev. Cancer. 2013; 13:83–96. [PubMed: 23303139]
9. Shangary S, Wang S. Small-molecule inhibitors of the MDM2-p53 protein-protein interaction to reactivate p53 function: a novel approach for cancer therapy. Annu. Rev. Pharmacol. Toxicol. 2009; 49:223–241. [PubMed: 18834305]
10. Reyes-Turcu FE, Ventii KH, Wilkinson KD. Regulation and cellular roles of ubiquitin-specific deubiquitinating enzymes. Annu. Rev. Biochem. 2009; 78:363–397. [PubMed: 19489724]
11. Komander D, Clague MJ, Urbe S. Breaking the chains: structure and function of the deubiquitinases. Nat. Rev. Mol. Cell. Biol. 2009; 10:550–563. [PubMed: 19626045]
12. Sun SC. Deubiquitylation and regulation of the immune response. Nat. Rev. Immunol. 2008; 8:501–511. [PubMed: 18535581]
13. Fraile JM, Quesada V, Rodriguez D, Freije JM, Lopez-Otin C. Deubiquitinases in cancer: new functions and therapeutic options. Oncogene. 2012; 31:2373–2388. [PubMed: 21996736]
14. Harhaj EW, Dixit VM. Regulation of NF-kappaB by deubiquitinases. Immunol. Rev. 2012; 246:107–124. [PubMed: 22435550]
15. Baker RT, Wang XW, Woollatt E, White JA, Sutherland GR. Identification, functional characterization, and chromosomal localization of USP15, a novel human ubiquitin-specific protease related to the UNP oncoprotein, and a systematic nomenclature for human ubiquitin-specific proteases. Genomics. 1999; 59:264–274. [PubMed: 10444327]
16. Vos RM, Altreuter J, White EA, Howley PM. The ubiquitin-specific peptidase USP15 regulates human papillomavirus type 16 E6 protein stability. J. Virol. 2009; 83:8885–8892. [PubMed: 19553310]
17. Inui M, et al. USP15 is a deubiquitylating enzyme for receptor-activated SMADs. Nat. Cell. Biol. 2011; 13:1368–1375. [PubMed: 21947082]
18. Eichhorn PJ, et al. USP15 stabilizes TGF-beta receptor I and promotes oncogenesis through the activation of TGF-beta signaling in glioblastoma. Nat. Med. 2012; 18:429–435. [PubMed: 22344298]
19. Hetfeld BK, et al. The zinc finger of the CSN-associated deubiquitinating enzyme USP15 is essential to rescue the E3 ligase Rbx1. Curr. Biol. 2005; 15:1217–1221. [PubMed: 16005295]
20. Wakil AE, Wang ZE, Ryan JC, Fowell DJ, Locksley RM. Interferon gamma derived from CD4(+) T cells is sufficient to mediate T helper cell type 1 development. J. Exp. Med. 1998; 188:1651–1656. [PubMed: 9802977]
21. Smith-Garvin JE, Koretzky GA, Jordan MS. T cell activation. Annu. Rev. Immunol. 2009; 27:591–619. [PubMed: 19132916]
22. Kiani A, et al. Regulation of interferon-gamma gene expression by nuclear factor of activated T cells. Blood. 2001; 98:1480–1488. [PubMed: 11520798]
23. Macian F. NFAT proteins: key regulators of T-cell development and function. Nat. Rev. Immunol. 2005; 5:472–484. [PubMed: 15928679]
24. Yoeli-Lerner M, et al. Akt blocks breast cancer cell motility and invasion through the transcription factor. NFAT. Mol. Cell. 2005; 20:539–550. [PubMed: 16307918]
25. Harper S, Besong TM, Emsley J, Scott DJ, Dreveny I. Structure of the USP15 N-terminal domains: a beta-hairpin mediates close association between the DUSP and UBL domains. Biochemistry. 2011; 50:7995–8004. [PubMed: 21848306]
26. Kitagaki J, Agama KK, Pommier Y, Yang Y, Weissman AM. Targeting tumor cells expressing p53 with a water-soluble inhibitor of Hdm2. Mol. Cancer Ther. 2008; 7:2445–2454. [PubMed: 18723490]
27. Manfredi JJ. The Mdm2-p53 relationship evolves: Mdm2 swings both ways as an oncogene and a tumor suppressor. Genes Dev. 2010; 24:1580–1589. [PubMed: 20679392]

28. Vassilev LT, et al. In vivo activation of the p53 pathway by small-molecule antagonists of MDM2. Science. 2004; 303:844–848. [PubMed: 14704432]
29. Ovaa H, et al. Activity-based ubiquitin-specific protease (USP) profiling of virus-infected and malignant human cells. Proc. Natl. Acad. Sci. U S A. 2004; 101:2253–2258. [PubMed: 14982996]
30. Take Y, Kumano M, Teraoka H, Nishimura S, Okuyama A. DNA-dependent protein kinase inhibitor (OK-1035) suppresses p21 expression in HCT116 cells containing wild-type p53 induced by adriamycin. Biochem. Biophys. Res. Commun. 1996; 221:207–212. [PubMed: 8619835]
31. Cheok CF, Kua N, Kaldis P, Lane DP. Combination of nutlin-3 and VX-680 selectively targets p53 mutant cells with reversible effects on cells expressing wild-type p53. Cell Death. Differ. 2010; 17:1486–1500. [PubMed: 20203688]
32. Overwijk WW, Restifo NP. B16 as a mouse model for human melanoma. Curr. Protoc. Immunol. Chapter. 2001; 20 Unit 20 21.
33. Kennedy R, Celis E. Multiple roles for CD4+ T cells in anti-tumor immune responses. Immunol. Rev. 2008; 222:129–144. [PubMed: 18363998]
34. Li M, et al. Deubiquitination of p53 by HAUSP is an important pathway for p53 stabilization. Nature. 2002; 416:648–653. [PubMed: 11923872]
35. Kon N, et al. Inactivation of HAUSP in vivo modulates p53 function. Oncogene. 2010; 29:1270–1279. [PubMed: 19946331]
36. Loch CM, Strickler JE. A microarray of ubiquitylated proteins for profiling deubiquitylase activity reveals the critical roles of both chain and substrate. Biochim. Biophys. Acta. 2012; 1823:2069–2078. [PubMed: 22626734]
37. Vanneman M, Dranoff G. Combining immunotherapy and targeted therapies in cancer treatment. Nat. Rev. Cancer. 2012; 12:237–251. [PubMed: 22437869]
38. Montes de Oca Luna R, Wagner DS, Lozano G. Rescue of early embryonic lethality in mdm2-deficient mice by deletion of p53. Nature. 1995; 378:203–206. [PubMed: 7477326]
39. Chang M, et al. The ubiquitin ligase Peli1 negatively regulates T cell activation and prevents autoimmunity. Nat. Immunol. 2011; 12:1002–1009. [PubMed: 21874024]
40. Reiley WW, et al. Deubiquitinating enzyme CYLD negatively regulates the ubiquitin-dependent kinase Tak1 and prevents abnormal T cell responses. J. Exp. Med. 2007; 204:1475–1485. [PubMed: 17548520]
41. Sun S-C, Ganchi PA, Beraud C, Ballard DW, Greene WC. Autoregulation of the NF-κB transactivator Rel A (p65) by multiple cytoplasmic inhibitors containing ankyrin motifs. Proc. Natl. Acad. Sci. USA. 1994; 91:1346–1350. [PubMed: 8108414]
42. Hassink GC, et al. The ER-resident ubiquitin-specific protease 19 participates in the UPR and rescues ERAD substrates. EMBO Rep. 2009; 10:755–761. [PubMed: 19465887]
43. Lu Y, et al. Th9 cells promote antitumor immune responses in vivo. J. Clin. Invest. 2012; 122:4160–4171. [PubMed: 23064366]
44. Cvijic ME, Xiao G, Sun SC. Study of T-cell signaling by somatic cell mutagenesis and complementation cloning. J. Immunol. Methods. 2003; 278:293–304. [PubMed: 12957416]
45. Foulds KE, et al. Cutting edge: CD4 and CD8 T cells are intrinsically different in their proliferative responses. J. Immunol. 2002; 168:1528–1532. [PubMed: 11823476]
46. Edwards LA, et al. Inhibition of ILK in PTEN-mutant human glioblastomas inhibits PKB/Akt activation, induces apoptosis, and delays tumor growth. Oncogene. 2005; 24:3596–3605. [PubMed: 15782140]

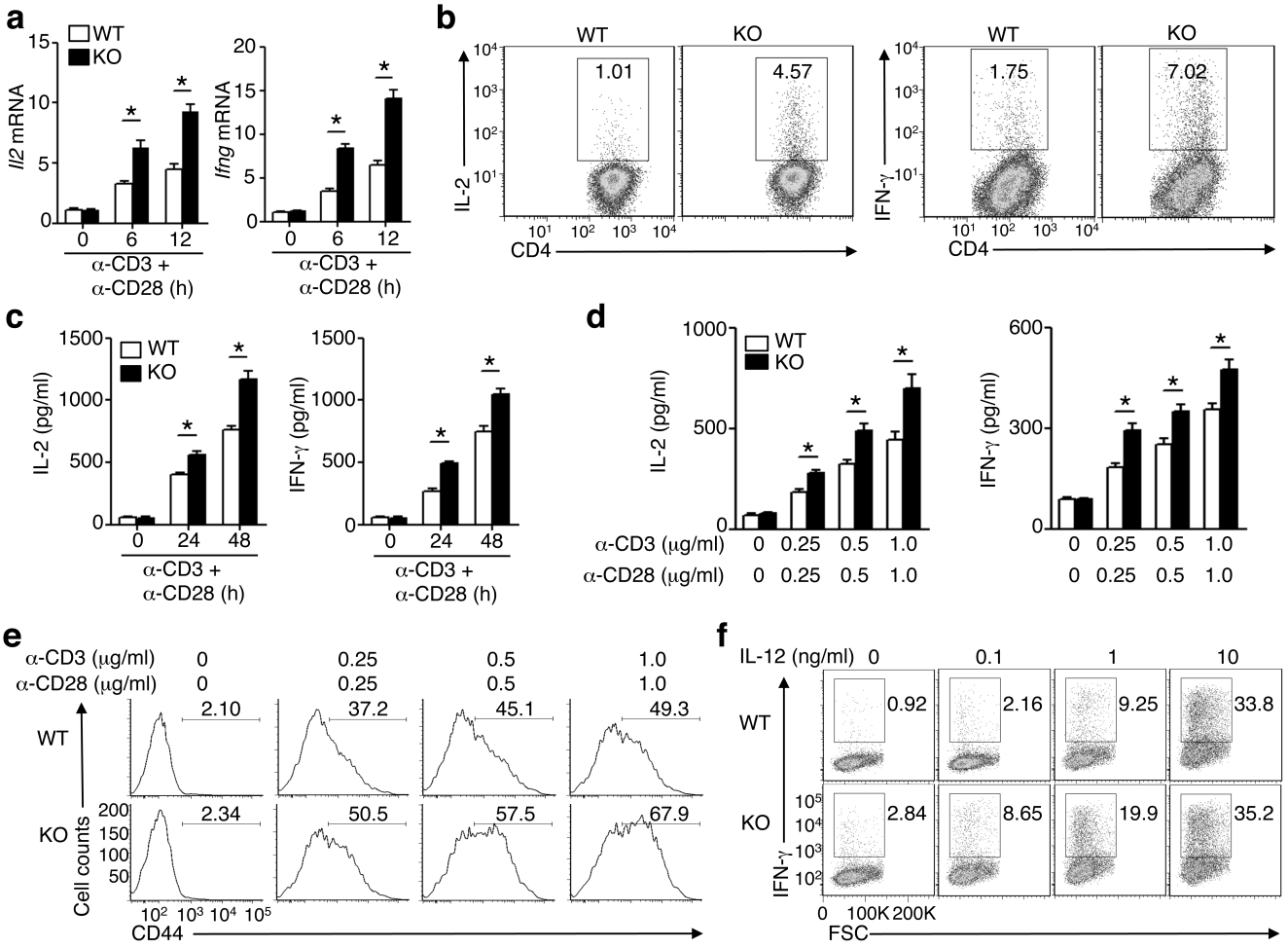


**Figure 1.**

Negative regulation of naïve CD4$^+$ T cell activation by USP15. (**a-c**) qRT-PCR analysis of *Il2* and *Ifng* mRNA (**a**, n=3), intracellular IFN-γ and IL-2 staining (**b**, n=5; showing a representative plot), and ELISA of secreted IL-2 and IFN-γ (**c**, n=3) of wild-type (WT) or *Usp15*$^{-/-}$ (KO) naïve CD4$^+$ T cells stimulated for various times (**a,c**) or 48 h (**b**). (**d,e**) ELISA of IL-2 and IFN-γ (**d**, n=3) and flow cytometric analysis of CD44 (**e**, n=3; showing a representative plot) in naïve CD4$^+$ T cells stimulated for 24 h with the indicated doses of anti-CD3 and anti-CD28. (**f**) Flow cytometric analysis of $T_H1$ cells, based on intracellular IFN-γ staining, in naïve wild-type and *Usp15*$^{-/-}$ CD4$^+$ T cells differentiated under Th1 conditions in the presence of the indicated doses of IL-12 (n=3; showing a representative plot). Bar graphs are mean ± s.e.m., and data are representative of four (**a-c**) or three (**d-f**) independent experiments. * P<0.05 (two-tailed unpaired *t*-test).

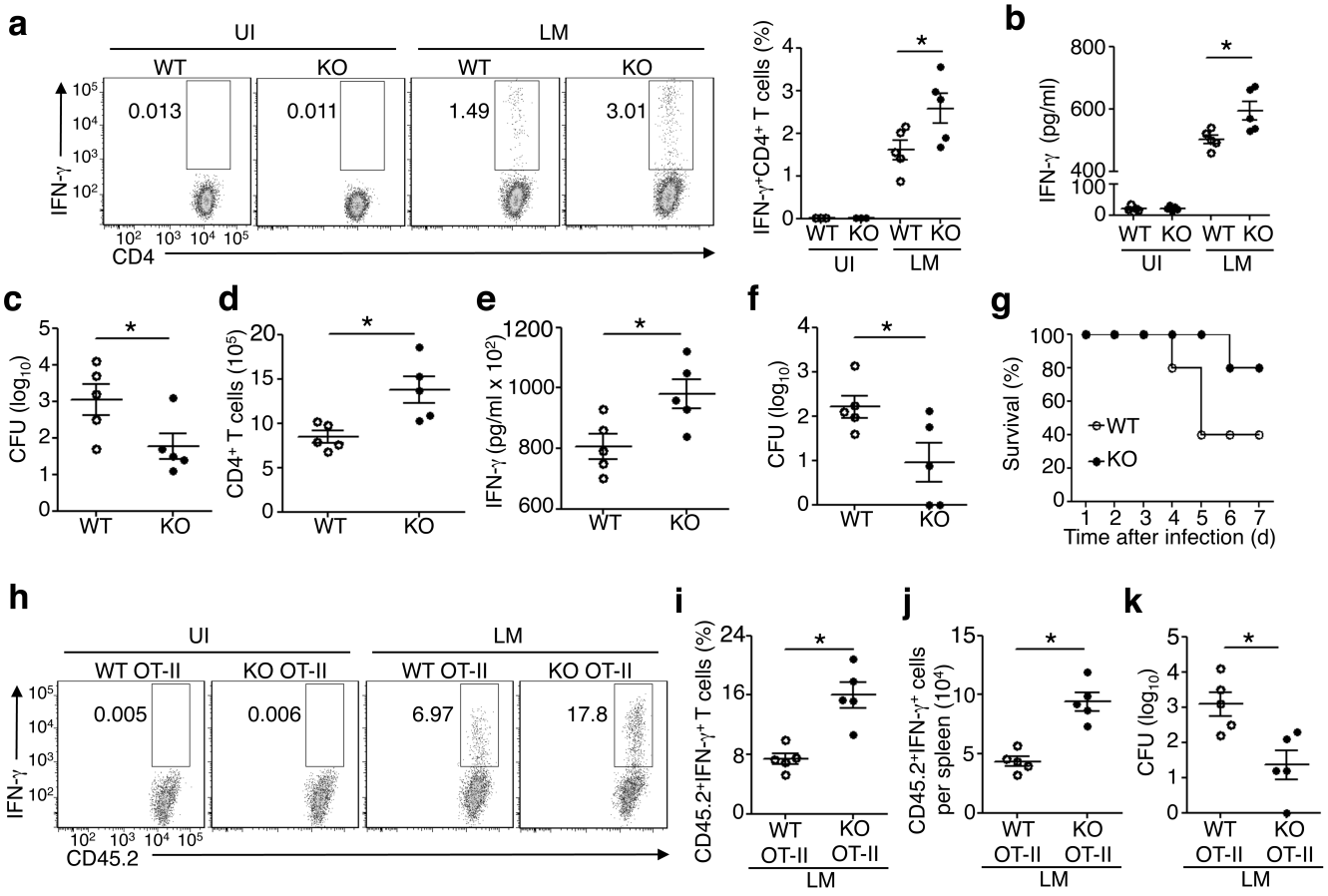


**Figure 2.**

USP15 deficiency promoted T cell responses to listeria infection. (**a-c**) Flow cytometric analysis of antigen (LLO)-specific IFN-γ-producing $CD4^+$ T cells in the spleen (**a**), ELISA of serum IFN-γ concentration (**b**), and liver *L. monocytogenes* titer (**c**) of uninfected and day 6 *L. monocytogenes*-infected mice (n=3 for uninfected and 5 for infected mice). (**d-g**) $CD4^+$ T cell number per spleen (**d**), serum IFN-γ concentration (**e**), liver *L. monocytogenes* titer (**f**), and survival curve (**g**) of *Tcrb/d*$^{-/-}$ mice reconstituted with wild-type (WT) or *Usp15*$^{-/-}$ (KO) naïve $CD4^+$ T cells along with wild-type $CD8^+$ T cells and then infected with *L. monocytogenes* for 4 (**d-e**) or 6 (**f**) days (n=5 for **e-f** and 10 for **g**). (**h-k**) ICS of the frequency (**h,i**) and absolute number (**j**) of the IFN-γ-producing OT-II ($CD45.2^+IFN\text{-}\gamma^+$) T cells and determination of liver *L. monocytogenes* titer (**k**) in day 6 LM-OVA-infected B6.SJL mice adoptively transferred with wild-type OT-II or *Usp15*$^{-/-}$ OT-II naïve $CD4^+$ T cells (n=5). UI, uninfected. LM, *L. monocytogenes* infected. Bacterial load is presented as colony-forming units (CFU) (**c,f,k**). Results are presented as mean ± s.e.m. or representative plots of multiple mice. Data are representative of four (**a-g**) or three (**h-k**) independent experiments. * P<0.05 (two-tailed unpaired *t*-test).

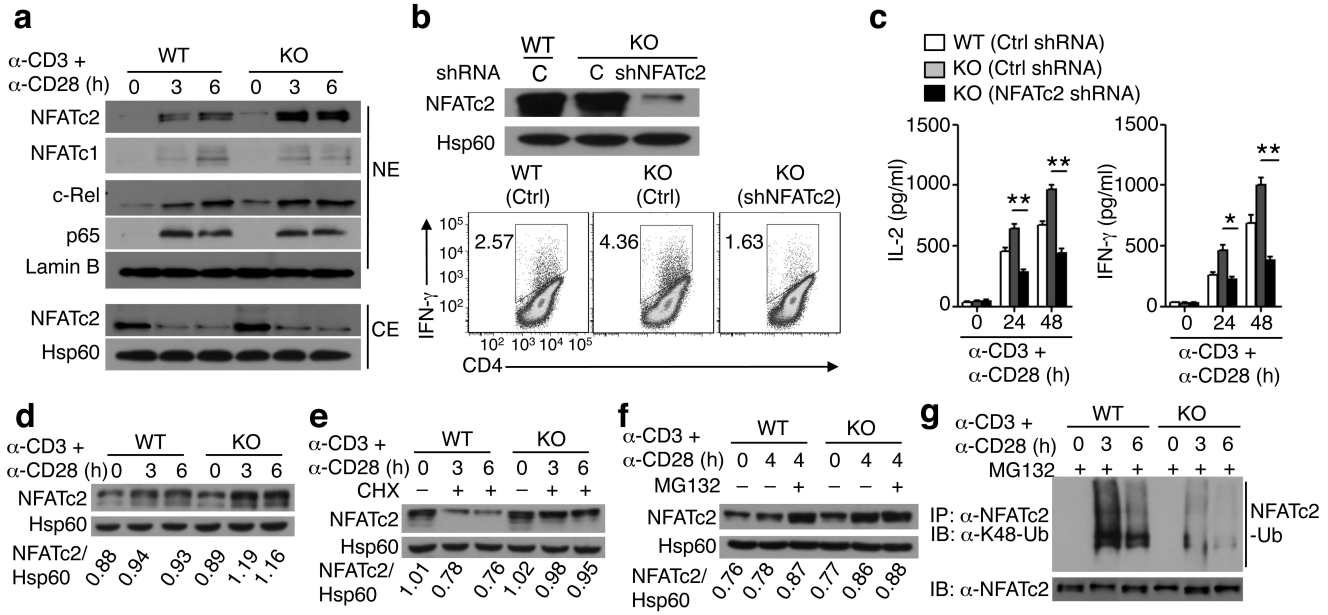


**Figure 3.**

USP15 deficiency inhibited the ubiquitin-dependent degradation of NFATc2 in activated T cells. (**a**) IB analysis of the indicated proteins in nuclear (NE) and cytoplasmic (CE) extracts of naive CD4$^+$ T cells stimulated with anti-CD3 plus anti-CD28. (**b,c**) wild-type (WT) or *Usp15*$^{-/-}$ (KO) bone marrow cells, transduced with a GFP-expressing lentiviral vector (pGIPZ) encoding a control (Ctrl) shRNA or an NFATc2 shRNA, were adoptively transferred into *Rag1*$^{-/-}$ mice. After 8 weeks, the chimeric mice were used for IB analysis of NFATc2 in sorted GFP$^+$ thymocytes (**b**, upper), IFN-γ ICS using naïve GFP$^+$CD4$^+$ splenic T cells stimulated for 72 hours with anti-CD3 plus anti-CD28 (**b**, lower; n=5, showing a representative plot), or ELISA of secreted IL-2 and IFN-γ in naïve GFP$^+$CD4$^+$ splenic T cells stimulated as indicated (**c**, n=3). * P<0.05; ** P<0.01 (two-tailed unpaired *t*-test). (**d-f**) IB analysis of NFATc2 in whole-cell extracts of naive CD4$^+$ T cells stimulated with anti-CD3 plus anti-CD28. Where indicated, CHX or MD132 was added (+) or not added (−) during the last 2 h. Densitometry-quantified protein bands, presented as NFATc2/Hsp60 ratios, are indicated underneath of the panels. (**g**) NFATc2 ubiquitination assays by first immunoprecipitating NFATc2 under denaturing conditions and then detecting the ubiquitinated NFATc2 using an anti-K48-ubiquitin antibody in naïve CD4$^+$ T cells stimulated in the presence of MG132 during the last 2 h. Data are representative of four (**a, d, g**) or three (**b, c, e, f**) independent experiments with at least three mice.

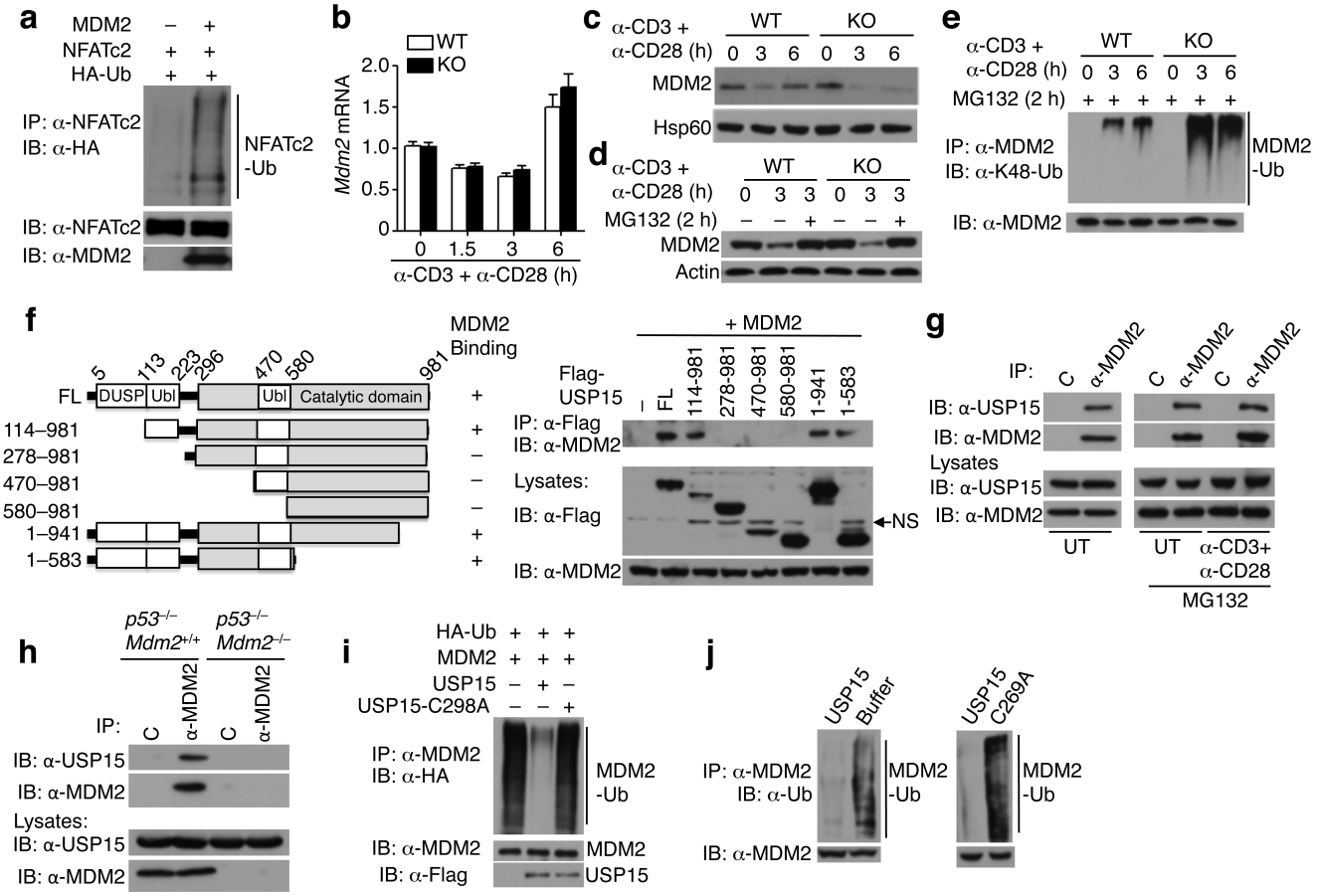


**Figure 4.**

USP15 mediated deubiquitination and stabilization of MDM2. (**a**) NFATc2 ubiquitination assays using HEK293 cells transfected with the indicated expression vectors. (**b**) qRT-PCR analysis of *Mdm2* mRNA relative level (normalized to the control *Actb*) (n=3). (**c-e**) MDM2 IB (**c,d**) and ubiquitination (**e**) analysis using whole-cell extracts of wild-type (WT) or *Usp15*$^{-/-}$ (KO) naïve CD4$^{+}$ T cells, stimulated with anti-CD3 plus anti-CD28. Where indicated, MG132 was added (+) or not added (−) during the last 2 h. (**f**) HEK293 cells were transfected with MDM2 along with Flag-tagged full length (FL) or mutant forms of USP15 and subjected to USP15-MDM2 co-IP (upper) or direct IB (lower) assays. A nonspecific band is indicated by NS. A schematic picture depicting the domains of USP15 is shown to the left. DUSP, domain in ubiquitin-specific proteases; Ubl, ubiquitin like domain. (**g**) wild-type naïve CD4$^{+}$ T cells were either untreated (UT) or stimulated for 2 h with anti-CD3 plus anti-CD28 and, where indicated, in the presence of MG132. Cell lysates were subjected to IP using anti-MDM2 or negative control (C) followed by IB detection of the co-precipitated MDM2 and USP15 (upper). Direct IB analysis was also included (lower). (**h**) Whole-cell lysates of naïve CD4$^{+}$ T cells isolated from *p53*$^{-/-}$ or *p53*$^{-/-}$*Mdm2*$^{-/-}$ mice were subjected to MDM2-USP15 co-IP and IB as in **g**. (**i**) MDM2 ubiquitination assays using HEK293 cells transfected with the indicated expression vectors. (**j**) Wild-type naïve CD4$^{+}$ T cells were stimulated for 2 h with anti-CD3 plus anti-CD28 in the presence of MG132. The MDM2–

ubiquitin conjugates were isolated by IP under denaturing conditions and incubated with buffer control or a commercial USP15 recombinant protein (left) or incubated with USP15 and USP15 mutant (C269A) proteins purified from transfected HEK293 cells (right). Ubiquitinated MDM2 was detected by IB. Data are representative of four (**a-e, g**) or three (**f, h-j**) independent experiments.

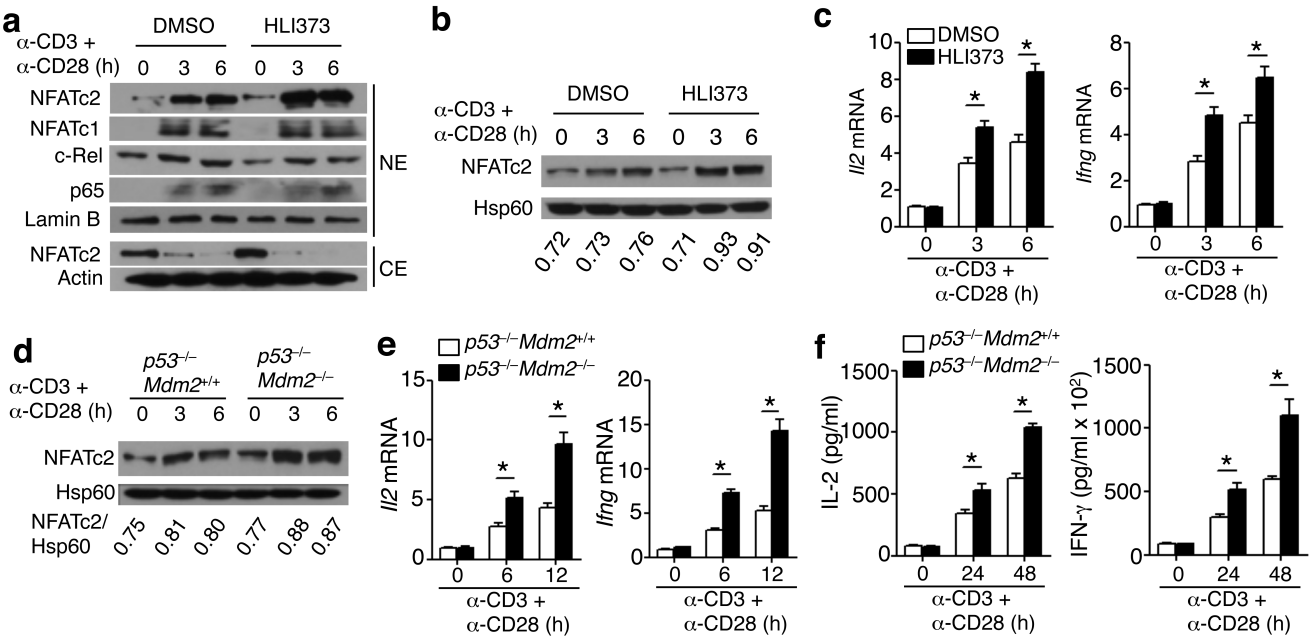


**Figure 5.**

MDM2 negatively regulated NFATc2 activation and cytokine induction in T cells in a p53-independent manner. (**a,b**) IB analyses using nuclear (NE) and cytoplasmic (CE) extracts (**a**) or whole-cell extracts (**b**) of wild-type naive CD4$^+$ T cells stimulated with anti-CD3 and anti-CD28 in the presence of DMSO or HIL373. Protein bands in **b** were quantified by densitometry and presented as NFATc2/Hsp60 ratios. (**c**) qRT-PCR analysis of *Il2* and *Ifng* mRNA relative level in wild-type naïve CD4$^+$ T cells, stimulated with anti-CD3 plus anti-CD28 in the presence of DMSO or HLI373 (n=3). (**d**) IB analysis of the indicated proteins in the whole-cell extracts of naive CD4$^+$ T cells from *p53*$^{-/-}$ and *p53*$^{-/-}$*Mdm2*$^{-/-}$ mice stimulated as indicated. (**e,f**) qRT-PCR analysis of *Il2* and *Ifng* mRNA (**e**) and ELISA of secreted IL-2 and IFN-γ (**f**) of anti-CD3/anti-CD28-stimulated naive CD4$^+$ T cells from *p53*$^{-/-}$ and *p53*$^{-/-}$*Mdm2*$^{-/-}$ mice (n=3). Data are representative of four (**a-c**) or three (**d-f**) independent experiments. * P<0.05 (two-tailed unpaired *t*-test).

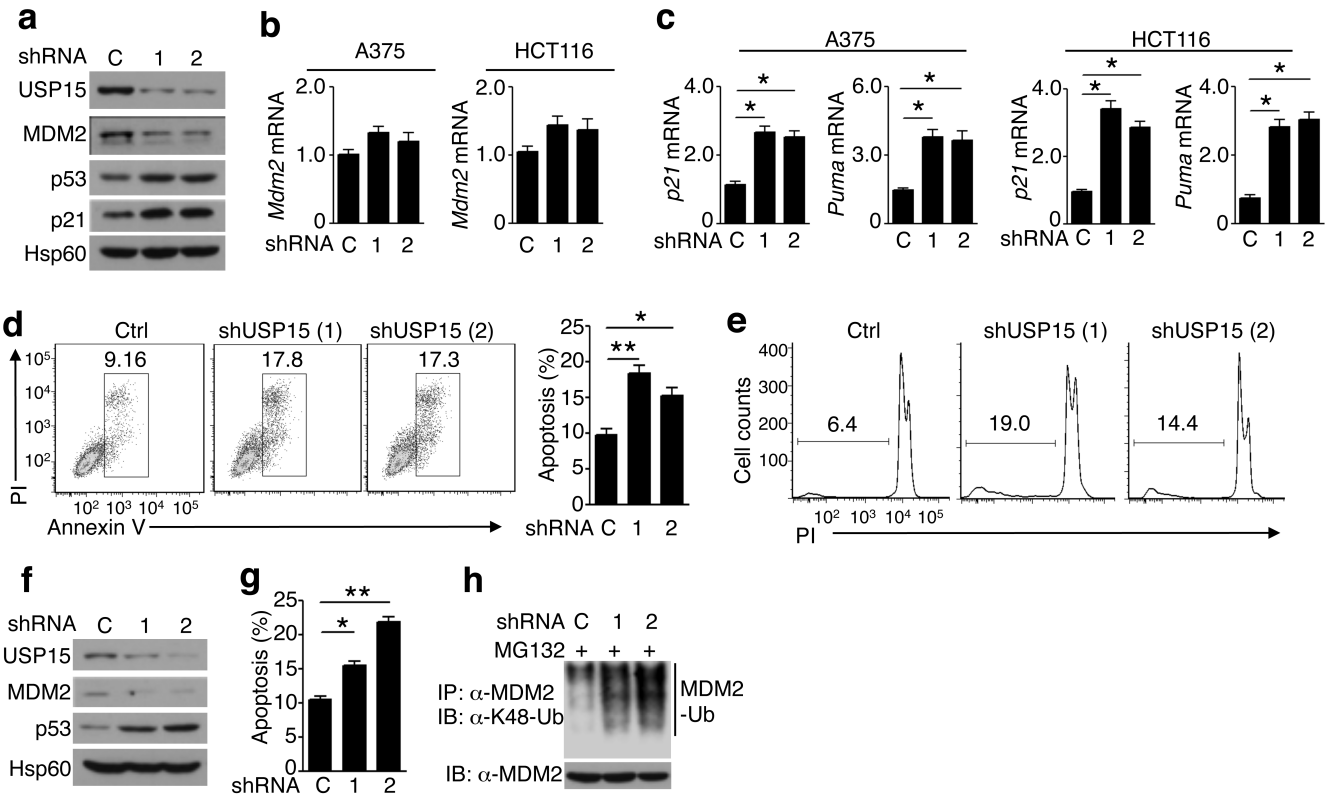


**Figure 6.**

USP15 stabilized MDM2 and negatively regulated p53-dependent gene expression and apoptosis in cancer cells. (**a**) IB analysis of A375 melanoma cells stably infected with a non-silencing control shRNA (C) or two different USP15 shRNAs. (**b,c**) qRT-PCR analysis of the indicated mRNAs relative to *Actb* in the control and USP15-knockdown A375 and HCT116 cells. (**d,e**) Analysis of spontaneous apoptosis of the control (Ctrl) and USP15-knockdown A375 cells based on annexin V staining (**d**) and content of nuclear PI staining (**e**). Percentage of apoptotic cells is indicated in the panels. (**f,g**) IB (**f**) and apoptosis (**g**) analysis of the control (C) and USP15-knockdown HCT116 cells. (**h**) MDM2 ubiquitination in the control (C) and USP15-knockdown A375 cells treated with MG132 for 2 h. Bar graphs are presented as mean ± s.e.m. Data are representative of five (**a, d, e, f, g**) or three (**b, c, h**) independent experiments. * P<0.05; ** P<0.01 (two-tailed unpaired *t*-test).

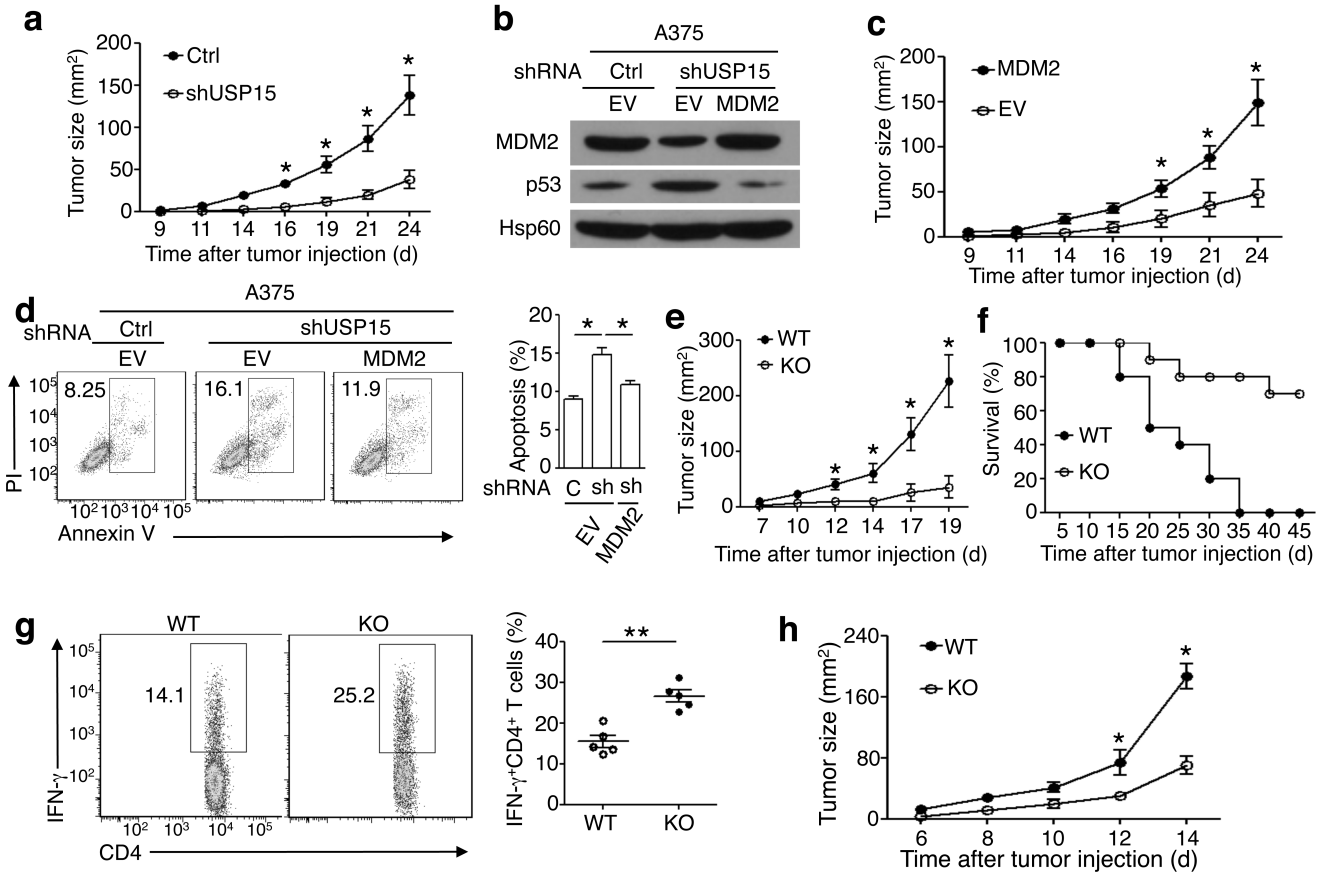


**Figure 7.**

USP15-mediated MDM2 stabilization promoted cancer cell survival and inhibited antitumor T-cell responses. (**a**) Growth curve of xenograft tumors in nude mice injected s.c. with control or USP15-silenced (shRNA (1)) A375 cells (n=7). (**b**) IB analysis of the indicated proteins in control (Ctrl) or USP15-silenced (shUSP15) A375 cells transduced with either an empty vector (EV) or MDM2 expression vector. (**c**) Growth curve of xenograft tumors in nude mice injected s.c. with USP15-silenced A375 cells infected with either MDM2 or an empty vector (EV) (n=5). (**d**) Flow cytometric analysis of spontaneous apoptosis of the control (Ctrl) and USP15-silenced (shUSP15 or sh) A375 cells transduced with MDM2 or empty vector (EV), showing a representative plot (number in the figure panels indicate percentage of apoptotic cells) and a summary graph (n=3). (**e,f**) Growth curve of tumors (**e**) and survival curve (**f**) of wild-type (WT) or *Usp15*$^{-/-}$ (KO) mice injected s.c. with B16 melanoma cells (n=10). (**g**) ICS of the frequency of IFN-γ-producing CD4$^{+}$ effector T cells among the tumor-infiltrating CD4$^{+}$ T cells (day 16 after B16 cell injection). Data are presented as a representative plot and a summary graph of multiple mice (n=5). (**h**) Growth curve of tumors in *Tcrb/d*$^{-/-}$ mice reconstituted with wild-type or *Usp15*$^{-/-}$ naïve CD4$^{+}$ T cells along with wild-type CD8$^{+}$ T cells and subsequently injected s.c. with B16 melanoma cells (n=10). Graphs are presented as mean ± s.e.m., and data are representative of four (**e-g**) or three (**a-d, h**) independent experiments. *P<0.05; **P<0.01 (two-tailed unpaired *t*-test).